the convergence and enforce the divergence-free velocity, the multigrid techique has been used to solve the pressure Poisson equation.

IV. Numerical Validation of Two-Dimensional Vortex Flows

The proposed RKCN four-step projection method is tested in computing the following two-dimensional unsteady flow of the decaying vortex, which has the exact solution as in Ref. 3. Computations are carried out in the domain $0 \le x, y \le \pi$. In the computation the uniform collocated meshes were used in the computation. On the boundaries the exact solution was imposed. The same CFL number is used for all of the tested algorithms. Figure 1 plots the maximum errors in u at different time level as a function of mesh refinement. Similar results were obtained for v. Figure 1 shows that the RKCN projection method is second-order temporal accuracy because the slope is greater than or equal to two.

V. Summary

1) A general second-order-temporal-accuracy formula of the projection method has been presented for unsteady incompressible Navier–Stokes equations based on the matrix analysis method, which has been further formed as the four- and three-step projection methods.

2) Some existing well-known projection methods have been analyzed based on the general four-step and three-step projection formulas; the SIMPLE method for unsteady flows has also been discussed.

3) The RKCN multistep projection methods have been developed. The three-stage low-storage Runge–Kutta technique is employed to explicitly update the convective term for stability and simplicity, and the semi-implicit Crank–Nicholson technique is employed to update the diffusion term for stability.

Acknowledgment

This work was made possible under the financial support of the Japan Society for the Promotion of Science.

References

[1]Harlow, F. H., and Welch, J. E., "Numerical Calculation of Time-Dependent Viscous Incompressible Flow of Fluid with Free Surface," *Physics of Fluids*, Vol. 8, No. 12, 1965, pp. 2182–2189.

[2]Chorin, A. J., "Numerical Solution of Navier–Stokes Equations," *Mathematics of Computation*, Vol. 22, No. 104, 1968, p. 745.

[3]Kim, J., and Moin, P., "Application of Fractional-Step Method to Incompressible Navier–Stokes Equations," *Journal of Computational Physics*, Vol. 59, No. 1, 1985, p. 108.

[4]Rai, M. M., and Moin, P., "Direct Simulation of Turbulent Flow Using Finite Difference Schemes," *Journal of Computational Physics*, Vol. 96, No. 1, 1991, p. 15.

[5]Perot, J. B., "An Analysis of the Fractional Step Method," *Journal of Computational Physics*, Vol. 108, No. 1, 1993, pp. 51–58.

[6]Perot, J. B., "Letter to the Editor: Comments on the Fractional Step Method," *Journal of Computational Physics*, Vol. 121, No. 1, 1995, pp. 190, 191.

[7]Bell, J. B., Colella, P., and Glaz, H. M., "A Second-Order Projection Method for the Incompressible Navier–Stokes Equations," *Journal of Computational Physics*, Vol. 85, No. 2, 1989, p. 257.

[8]Choi, H., and Moin, P., "Effects of the Computational Time Step on Numerical Solutions of Turbulent Flow," *Journal of Computational Physics*, Vol. 113, No. 1, 1994, pp. 1–4.

[9]Morinishi, Y., Lund, T. S., Vasilyev, O. V., and Moin, P., "Fully Conservative Higher Order Finite Difference Schemes for Incompressible Flow," *Journal of Computational Physics*, Vol. 143, No. 1, 1998, pp. 90–124.

[10]Dukowicz, J. K., and Dvinsky, A. S., "Approximation Factorization as a High Order Splitting for Implicit Incompressible Flow Equations," *Journal of Computational Physics*, Vol. 102, No. 2, 1992, pp. 336–347.

[11]Gresho, P., "On the Theory of Semi-Implicit Projection Methods for Viscous Incompressible Flow and Its Implementation via a Finite Element Method that also Introduce a Nearly Consistent Mass Matrix, Part 1: Theory," *International Journal of Numerical Methods in Fluids*, Vol. 11, No. 6, 1990, pp. 587–620.

[12]Patankar, S. V., *Numerical Heat Transfer and Fluid Flow*, McGraw–Hill, New York, 1980, pp. 79–137.

J. Kallinderis
Associate Editor

Atmospheric Stability Effects in Aircraft Near-Wake Modeling

Milton E. Teske*
Continuum Dynamics, Inc., Ewing, New Jersey 08618
and
Harold W. Thistle†
U.S. Department of Agriculture Forest Service, Morgantown, West Virginia 26505

Introduction

In an earlier Technical Note[1] the decay rate of aircraft vortices near the ground was developed from a series of aircraft flybys above tower grids instrumented with propeller anemometers. The experiments recovered an average decay rate for the vortices when aircraft were flying in an atmosphere whose stability was characterized by Richardson numbers no more negative than -0.20, where the Richardson number is defined as $Ri = (g/\Theta_0)(\mathrm{d}\Theta/\mathrm{d}z)/(\mathrm{d}u/\mathrm{d}z)^2$, where g is gravity (m/s^2), Θ_0 is the reference temperature (K), $\mathrm{d}\Theta/\mathrm{d}z$ is the background temperature gradient (K/m), and $\mathrm{d}u/\mathrm{d}z$ is the background velocity gradient (s^{-1}). It was found that $-(s/\Gamma_i)^2(\mathrm{d}\Gamma/\mathrm{d}t)_{t=0} = bqs/\Gamma_i = 0.051$, for an assumed exponential vortical decay of the form $\Gamma = \Gamma_i e^{-bqt/s}$, where Γ is the vortex circulation strength (m^2/s) as a function of time t (s), Γ_i is the initial vortex circulation strength at $t = 0$, b is the decay coefficient, q is the background turbulence level (m/s), and s is the aircraft semispan (m). This decay rate was then inserted into the U.S. Department of Agriculture Forest Service aerial application model AGDISP[2] and later into its regulatory version AgDRIFT®[3] (developed in cooperation with the Spray Drift Task Force and the U.S. Environmental Protection Agency). The vortical decay assumption improved near-wake model predictions in ground deposition and considerably improved comparisons with field data.[4]

The influence of atmospheric stability on atmospheric dispersion and hence deposition is well known.[5] In a recent review of published aerial field studies,[6] only nine of the 42 studies examined (conducted between 1967 and 1990) were classified as having taken place in neutral conditions (21.4%). In contrast, for the aerial field trials conducted by the Spray Drift Task Force atmospheric conditions were reported as either neutral or unstable for 97.2% of the trials,[7] with an average Richardson number of -0.05 and Richardson numbers as negative as -0.81. Thus, an extension of the near-wake model to include nonneutral (stable and unstable) atmospheric conditions would seem to be appropriate when making these data comparisons.

Atmospheric conditions enter the near-wake model in three ways: 1) the structure of the crosswind velocity profile; 2) the atmospheric background turbulence level; and 3) interaction with the strength, size, and behavior of the aircraft vortices. The crosswind velocity profile may be well approximated by the profile extension suggested by Panofsky[8] and Golder,[9] whereas the atmospheric background turbulence level can be parameterized with respect to Richardson number.[10,11] The effects of various atmospheric stability conditions on the behavior of the aircraft vortices form the subject of this Note.

Discussion

To examine atmospheric stability effects, calculations were made with the latest version of the second-order closure, invariant turbulence model as programmed in UNIWAKE. This model has

Received 14 September 2001; revision received 7 February 2002; accepted for publication 20 March 2002.

*Senior Associate, 34 Lexington Avenue. Member AIAA.
†Program Manager, 180 Canfield Street.

an extensive history,[12,13] including the addition of engine exhaust chemistry and late-wake effects.[14,15] In this application the model solves the three-dimensional steady Navier–Stokes equations for turbulent kinetic energy, temperature, and vorticity. The crossflow velocity field is found by solving a Poisson equation for the stream function, then differentiating to obtain the horizontal and vertical velocities.

The imposition of background velocity and temperature gradients enables the model to compute stable and unstable atmospheric effects on the aircraft vortices. These gradients are parameterized through the use of the Pasquill stability classification scheme,[16] which classifies the surface radiation regime that largely controls atmospheric stability in the surface layer. The scheme defines six categories, based on estimates of incoming solar radiation intensity (daytime), percent cloud cover (nighttime), and wind speed. This simple scheme allows stability to be approximately classified, with minimal observations, into class A, strongly unstable; class B, moderately unstable; class C, slightly unstable; class D, neutral; class E, slightly stable; and class F, moderately stable.

Three calculations were undertaken, for strongly unstable, neutral, and moderately stable stability conditions, assuming model defaults[3] for aerial application from an Air Tractor AT-401, with a flying height of 3 m and a headwind of 1 m/s (an AT-401 has $s = 7.47$ m, a typical flying speed $U_\infty = 53.64$ m/s, and $\Gamma_i = 34.56$ m^2/s). The background velocity gradient establishes a consistent level of background turbulence for each calculation because it can be shown[13] for neutral atmospheric conditions that $q = \sqrt{2}\Lambda(\mathrm{d}u/\mathrm{d}z)$, where Λ is the turbulent macroscale length and the velocity gradient is approximated by a logarithmic profile. Nonneutral stability conditions modify the turbulence level, depending on solar radiation level,[17] which in turn modifies the background velocity gradient, the Richardson number, and the background temperature gradient. The three cases can be summarized as shown in Table 1. Model calculations were undertaken on a grid spanning a horizontal distance of $y/s = 12$ and a vertical distance of $z/s = 36$, with a uniform grid spacing of $\Delta y/s = \Delta z/s = 0.05$.

Results are presented in Fig. 1 for the three cases considered. (For a headwind the solution is symmetrical across the centerline of the aircraft, and only one side of the aircraft wake is computed and plotted.) Some observations are as follows:

1) In the neutral and moderately stable cases the vorticity tends to remain within its original oval shape, whereas in the strongly unstable case the vorticity disperses rapidly. A comparison of maximum vorticity is given in Fig. 2, where it can be seen that vortical strength decays more rapidly as the atmosphere becomes more unstable.

2) All three cases predict similar vertical movement of the vortex core, with the core descending more slowly as the atmosphere becomes more unstable: at $tU_\infty/s = 215.4$ the core has descended to $z/s = -1.924$ (moderately stable), -1.788 (neutral), and -1.648 (strongly unstable).

3) In the strongly unstable case the vorticity is quickly dispersed beyond its original vortex core, whereas in the moderately stable case waves break from the top of the vortex and move away from the aircraft centerline. (The computational domain is much larger than shown here to avoid stability effects generated near its edges.)

4) The structure of the vortex core is difficult to describe for the strongly unstable case; however, for the moderately stable case (before wave breaking began) the vertical scale flattens in comparison with the neutral case. In a stable layer vertically displaced air will tend to return to its vertical level of origin, with the potential of causing vortices to become horizontally elongated, while damping turbulent energy and resisting vertical mixing.

5) The distance between the vortex cores (across the centerline) remains fairly constant for the neutral and moderately stable cases, consistent with previous findings.[18] The strongly unstable case is clearly affected by the increased background turbulence level. The competing effects present in the problem description (temperature turning over within the vortex, vortex diffusion damped vertically in the moderately stable case and stretched vertically in the strongly unstable case, dispersion effects caused by increased or diminished turbulence level) appear to be simulated correctly.

The vortical decay rates exhibited in Fig. 2 recover a decay coefficient 2.45 times that of neutral for the strongly unstable case and

Table 1 Background gradient summary

Stability class	q/U_∞	$(s/U_\infty)(\mathrm{d}u/\mathrm{d}z)$	Ri	$(s/\Theta_0)(\mathrm{d}\Theta/\mathrm{d}z)$
Strongly unstable	0.004555	0.03221	−0.25	−0.01018
Neutral	0.003066	0.02168	0.0	0.0
Moderately stable	0.002168	0.01533	0.15	0.001384

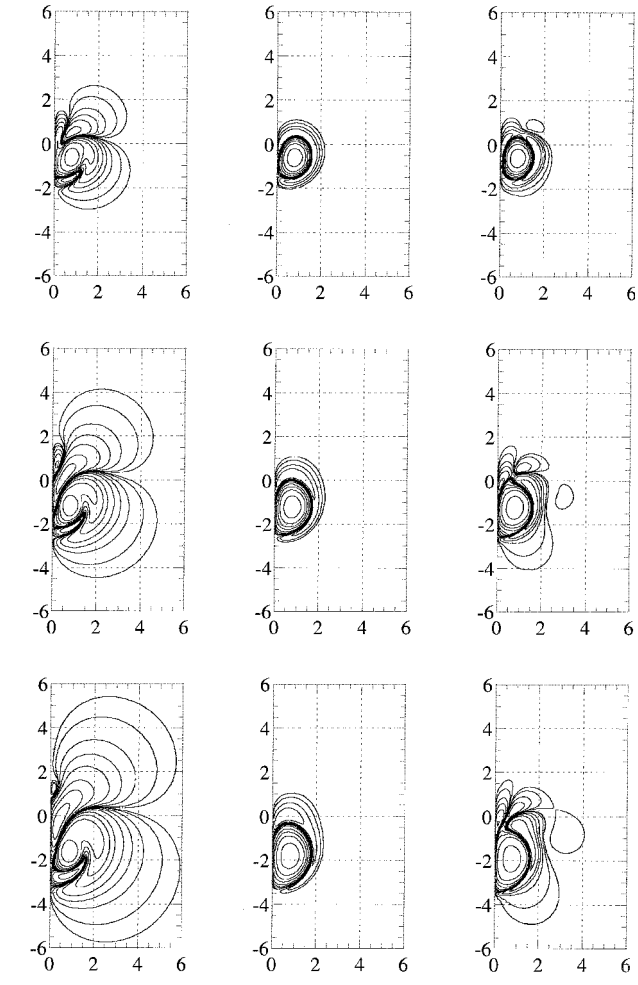

Fig. 1 Isopleths of vorticity Ω (s^{-1}) for one side of the aircraft wake, for strongly unstable (left column), neutral (center column), and moderately stable (right column) stability categories: $tU_\infty/s = 71.8$ with $\Omega_{\max}s/U_\infty = 0.11749, 0.15619$, and 0.16294, respectively (top row); $tU_\infty/s = 143.6$ with $\Omega_{\max}s/U_\infty = 0.06288$, 0.10800, and 0.11812, respectively (middle row); and $tU_\infty/s = 215.4$ with $\Omega_{\max}s/U_\infty = 0.03824$, 0.08526, and 0.09879, respectively (bottom row).

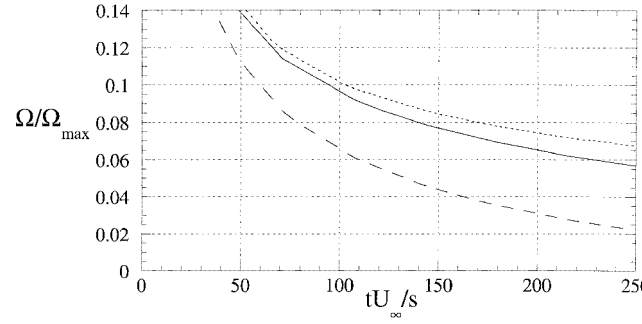

Fig. 2 Comparison of vortical decay as a function of time after vortex release, for strongly unstable (– – –), neutral (——), and moderately stable (· · · ·) stability categories.

0.98 times that of neutral for the moderately stable case. These trends suggest greater vortical dispersion in an unstable atmosphere and less (or about the same) dispersion in a stable atmosphere, relative to neutral conditions.

Conclusions

Atmospheric stability effects in aircraft near-wake modeling can be simulated by vortical decay rates predicted by UNIWAKE. Inclusion of these effects into AGDISP and AgDRIFT will extend the capabilities of both models to handle general atmospheric conditions.

References

[1]Teske, M. E., Bilanin, A. J., and Barry, J. W., "Decay of Aircraft Vortices near the Ground," *AIAA Journal*, Vol. 31, No. 8, 1993, pp. 1531–1533.

[2]Bilanin, A. J., Teske, M. E., Barry, J. W., and Ekblad, R. B., "AGDISP: The Aircraft Spray Dispersion Model, Code Development and Experimental Validation," *Transactions of the American Society of Agricultural Engineers*, Vol. 32, No. 1, 1989, pp. 327–334.

[3]Teske, M. E., Bird, S. L., Esterly, D. M., Curbishley, T. B., Ray, S. L., and Perry, S. G., "AgDRIFT®: A Model for Estimating Near-Field Spray Drift from Aerial Applications," *Environmental Toxicology and Chemistry*, Vol. 21, No. 3, 2002, pp. 659–671.

[4]Bird, S. L., Perry, S. G., Ray, S. L., and Teske, M. E., "Evaluation of the AGDISP Aerial Spray Algorithms in the AgDRIFT® Model," *Environmental Toxicology and Chemistry*, Vol. 21, No. 3, 2002, pp. 672–681.

[5]Thistle, H. W., "The Role of Stability in Fine Droplet Dispersion in the Atmosphere: A Review of Physical Concepts," *Transactions of the American Society of Agricultural Engineers*, Vol. 43, No. 6, 2001, pp. 1409–1413.

[6]Bird, S. L., "A Compilation of Aerial Spray Drift Field Study Data for Low-Flight Agricultural Application of Pesticides," *Agrochemical Environmental Fate*, edited by M. L. Leng, E. M. K. Leovey, and P. L. Zubkoff, Lewis Publishers, Boca Raton, FL, 1995, pp. 195–207.

[7]Bird, S. L., Esterly, D. M., and Perry, S. G., "Off-Target Deposition of Pesticides from Agricultural Aerial Spray Applications," *Journal of Environmental Quality*, Vol. 25, No. 5, 1996, pp. 1095–1104.

[8]Panofsky, H. A., "Determination of Stress from Wind and Temperature Measurements," *Quarterly Journal of the Royal Meteorological Society*, Vol. 89, No. 1, 1963, pp. 85–94.

[9]Golder, D., "Relations Among Stability Parameters in the Surface Layer," *Boundary-Layer Meteorology*, Vol. 3, No. 1, 1972, pp. 47–58.

[10]Lewellen, W. S., and Teske, M. E., "Prediction of the Monin-Obukhov Similarity Functions from an Invariant Model of Turbulence," *Journal of the Atmospheric Sciences*, Vol. 30, No. 7, 1973, pp. 1340–1345.

[11]Donaldson, C. duP., "Construction of a Dynamic Model of the Prediction of Atmospheric Turbulence and the Dispersal of Atmospheric Pollutants," *American Meteorological Society Workshop on Micrometeorology*, edited by D. A. Haugen, Science Press, Boston, 1973, pp. 313–390.

[12]Bilanin, A. J., Teske, M. E., and Williamson, G. G., "Vortex Interactions and Decay in Aircraft Wakes," *AIAA Journal*, Vol. 15, No. 2, 1977, pp. 250–260.

[13]Bilanin, A. J., Teske, M. E., and Hirsh, J. E., "Neutral Atmospheric Effects on the Dissipation of Aircraft Vortex Wakes," *AIAA Journal*, Vol. 16, No. 9, 1978, pp. 956–961.

[14]Quackenbush, T. R., Teske, M. E., and Bilanin, A. J., "Computation of Wake/Exhaust Mixing Downstream of Advanced Transport Aircraft," AIAA Paper 93-2944, July 1993.

[15]Quackenbush, T. R., Teske, M. E., and Bilanin, A. J., "Dynamics of Exhaust Plume Entrainment in Aircraft Vortex Wakes," AIAA Paper 96-0747, Jan. 1996.

[16]Pasquill, F., "The Estimation of the Dispersion of Windborne Material," *Meteorological Magazine*, Vol. 90, No. 1, 1961, pp. 33–49.

[17]Bjorklund, J. R., Bowman, C. R., and Dumbauld, R. K., "User's Manual for the Mesoscale Wind Field Model Statistical Evaluation Computer Program MWMSE," H. E. Cramer, Inc., TR-84-347-01, Salt Lake City, UT, June 1984.

[18]Hecht, A. M., Bilanin, A. J., and Hirsh, J. E., "Turbulent Trailing Vortices in Stratified Fluids," *AIAA Journal*, Vol. 19, No. 6, 1981, pp. 691–698.

A. Plotkin
Associate Editor

One-Dimensional Numerical Study of Compressible Flow Ejector

Sam Han* and John Peddieson Jr.†
Tennessee Technological University, Cookeville, Tennessee 38505

Nomenclature

A	=	ejector mixing tube cross-sectional area, m^2
e	=	internal energy per unit mass, J/kg
M	=	Mach number
m'''_{inj}	=	primary flow mass injection rate per unit volume, kg/s · m^3
$\dot{m}$	=	mass flow rate, kg/s
p	=	static pressure, Pa
T	=	temperature, K
u	=	velocity, m/s

Subscripts

e	=	mixing tube exit
i	=	mixing tube inlet
inj	=	primary flow injection condition
p	=	primary flow
s	=	secondary flow
t	=	stagnation condition

Superscript

*	=	primary flow nozzle throat or previous iteration value

Introduction

COMPRESSIBLE flow ejectors are widely used in many engineering applications, and various analysis tools have been developed over the years to analyze them. The simplest approach is the control volume method, in which steady one-dimensional mass, momentum, and energy equations are used.[1–6] In control volume analysis, flow conditions are known only at the boundaries of an ejector, as shown in Fig. 1. There are four distinctive ejector flow regimes[1]: supersonic (S), saturated supersonic (SS), mixed (M), and mixed with separation (MS). In the S regime, the secondary flow is choked at a location c, which is called "Fabri or aerodynamic choking" (Fig. 1). In the SS regime, the secondary flow chokes at the area minimum in the secondary flow path. In the M regime, the secondary flow remains subsonic at the inlet, and there is no Fabri choking inside the mixing tube. In the MS regime, the primary flow stagnation pressure is so low that the primary flow separates in the diverging part of the primary flow nozzle. Fabri's model used four sets of equations covering the four flow regimes just discussed. Addy[2] extended Fabri's model further and developed more systematic methods of selecting these flow regimes. Another control-volume-based method assumes the exit flow Mach number and calculates the secondary flow inlet conditions by iteration.[6] In this approach, a critical assumption is the existence of static pressure equilibrium between the primary and the secondary flow somewhere downstream from the mixing tube inlet. The Fabri choking assumption is not used in this approach, and some researchers have pointed out that this method fails for cases in which the Fabri choking assumption is needed.[2]

Received 24 September 2001; revision received 19 February 2002; accepted for publication 8 April 2002.

*Professor, Department of Mechanical Engineering; shan@tntech.edu. Member AIAA.

†Professor, Department of Mechanical Engineering.